JZAR JOURNAL OF ZOO AND AQUARIUM RESEARCH
www.jzar.org

Research article

Structure and mechanical properties of normal and anomalous teeth in the sand tiger shark *Carcharias taurus*

Ludwig Jansen van Vuuren[1*], Carolina Loch[1], Jules A. Kieser[1†], Keith C. Gordon[2] and Sara J. Fraser[2]

[1]Sir John Walsh Research Institute, Faculty of Dentistry, University of Otago, Dunedin 9054, New Zealand
[2]MacDiarmid Institute of Advanced Materials and Nanotechnology, Chemistry Department, University of Otago, Dunedin, New Zealand
**Correspondence: Ludwig Jansen van Vuuren, Department of Oral Rehabilitation, School of Dentistry, PO Box 647, Dunedin 9054, New Zealand; e-mail: ludwig.jvv@otago.ac.nz*
†Deceased

Keywords:
Chondrichthyes, enameloid microstructure, fluoroapatite, nanoindentation, Raman spectroscopy

Article history:
Received: 27 March 2014
Accepted: 9 April 2015
Published online: 30 April 2015

Abstract
This study reports and characterises an anomalous condition in teeth of captive sand tiger sharks *Carcharias taurus*. Abnormal shed teeth from captive sand tiger sharks which were soft to the touch were structurally and chemically characterised and compared to the structure and composition of normal teeth of the species. Normal specimens exhibited the expected tooth morphology with a well-developed tooth crown consisting of a central cusp and two lateral cusplets with smooth and sharp margins, while in the anomalous specimens the crown height was much reduced and the overall shape did not follow this pattern. Lateral cusplets were also considerably reduced in size and with blunt margins. Scanning electron images showed a distinct absence of crystalline structures in the anomalous specimens. Raman microscopy analysis confirmed the low volume of fluoroapatite in the outer layers of the anomalous teeth, while the composition of the inner layers corresponding to dentine was comparable to the normal tooth specimens. Nanoindentation-derived mechanical properties showed significant differences between the anomalous and normal teeth. The mean values for enameloid elastic modulus and hardness of all three normal teeth were 75.92±3.4 GPa and 3.27±0.41 GPa, respectively. On the other hand, mean values of elastic modulus and hardness for anomalous teeth were 7.81±3.27 GPa and 0.39±0.25 GPa, respectively. However, mechanical property values of the dentine of normal and anomalous teeth were similar. The mean values of dentine elastic modulus and hardness of the normal teeth were 25.66±2.14 GPa and 0.89±0.01 GPa, respectively, while mean values for the anomalous teeth were 25.34±1.54 GPa and 0.83±0.03 GPa. Although the morphological, mechanical and chemical differences between the normal and anomalous teeth are quite evident, establishing the causes of this condition are not possible at this stage.

Introduction

Elasmobranchs (sharks, rays and skates) typically have numerous teeth that are arranged in rows and are frequently replaced. Shark teeth are complex biocomposites, consisting of an inner core of dentine overlaid by a layer of enameloid. The purpose of this system is to absorb and distribute stresses during feeding, with the highly mineralised, hard enameloid coating supporting cutting and slicing loads, and the bulky, less mineralised, more elastic dentine resisting cracks propagating from the enameloid (Imbeni et al. 2005; Xue et al. 2013). This bi-layered structure is interfaced by the enamel–dentinal junction (EDJ), which is a complex hybrid entity representing a thin, but gradual interface, with characteristics transiting from those of dentine to those of enameloid (Chan et al. 2011, Dusevich et al. 2012). The EDJ has remarkable mechanical properties of high fracture toughness and crack resistance (Chan et al. 2011). Enameloid is a complex biomaterial, with elongated mineral crystallites forming a biological apatite bound by polymeric proteins and peptide chains. However, in contrast to mammalian enamel, the biomineral phase of enameloid consists of fluoroapatite ($Ca_2(PO_4)F$), which confers on it a higher elastic modulus than hydroxyapatite (Enax et al. 2012; Gardner et al. 1992; Whitenack et al. 2011).

While numerous studies have focused either on the evolutionary aspects of pattern formation in the replacement of shark teeth (for review see Smith et al. 2013), or on the dental morphology of extant and extinct forms (Gillis and Donoghue

2007; Goto 1991; Maisey 1982; Mertinene 1982), few have addressed the relationship between mechanical behaviour and tooth shape. Recently, Whitenack et al. (2010, 2011) performed finite element analysis to visualise stress distributions in fossil and living shark teeth under different feeding modalities such as puncturing, cutting and holding of prey. These authors showed clearly that shark teeth were structurally strong in puncturing, with stress concentrations focused on the cusp apex, and that these were much higher than those recorded for cutting or holding. In other words, despite high stress concentrations at cusp apices, shark teeth appeared to be well designed to resist fracture during puncturing of prey. These biomechanical studies have often relied on shed teeth of sharks kept in public aquaria.

The sand tiger shark *Carcharias taurus* has become a commonly displayed species in aquaria throughout the world due to its large size and menacing appearance, contrasted with its docile behaviour (Huber et al. 2013). This has allowed the study and documentation of pathological conditions affecting the skeleton and teeth of these animals. Skeletal anomalies such as spinal deformities, along with a variety of other abnormalities including curled pectoral fins, gingival hyperplasia and permanently protruded upper jaws, have been diagnosed in wild and captive sharks (Anderson et al. 2012; Hoenig and Walsh 1983; Huber et al. 2013; Preziosi et al. 2006). The incidence of spinal deformities of varying severity is reasonably high in captive sharks, affecting approximately 35% of sand tigers held in public aquaria (Anderson et al. 2012; Huber et al. 2013). However, skeletal anomalies have never been documented in wild *C. taurus* (Anderson et al. 2012). The aetiology of these anomalies has been linked with trauma induced during capture, irregular swimming behaviour and nutritional deficiencies. In particular, affected animals showed low serum concentrations of vitamins C and E, potassium and zinc, factors that are known to affect the skeletal mineralisation process in other vertebrates (Anderson et al. 2012).

Cases of anomalous teeth have been recorded in many recent and fossil sharks, involving individual teeth or the entire tooth file (Balbino and Antunes 2007; Becker et al. 2000). These include shape anomalies, asymmetries, missing or misshaped cusps, atypical protuberances, perforations, abnormal root structures and uncharacteristic bent or twisted tooth crowns. These anomalies have been related to disease and mutation; however trauma on the tooth-forming tissues from diet or feeding damage seems to be the main cause of dental anomalies in sharks (Balbino and Antunes 2007; Becker et al. 2000).

We were recently presented with a number of abnormal teeth from captive sand tiger sharks *C. taurus*, in which the characteristic morphology had been lost and which were soft to the touch. The questions now arise, how did these teeth differ in their microstructure and chemical composition, and secondly, how did this affect their mechanical properties? In this study, we used scanning electron microscopy (SEM), Raman spectroscopy and nanoindentation analyses to address these questions.

Methods

Specimen preparation

The two anomalous shed teeth analysed in this study were gathered from the tank of captive specimens in Kelly Tarlton's Sea Life Aquarium in Auckland, New Zealand. One typical normal shed tooth of a sand tiger shark was also obtained from the tank of captive specimens of Kelly Tarlton's Sea Life Aquarium and one from the Sydney Sea Life Aquarium, Australia. One tooth from a wild specimen was obtained from the Natal Sharks Board, Durban, South Africa. Prior to testing, all teeth were stored in 10% buffered formalin. Tooth surfaces were cleaned with ethanol and teeth were then embedded in epoxy resin (Epofix™ Cold-Setting Embedding Resin, Struers, Copenhagen, Denmark) using silicon moulds. After setting for 24 hours, specimens were longitudinally sectioned in the perpendicular plane (Fig. 1) using a diamond grit blade with a low speed cutting saw (DTQ-5, Laizhou Huayin Testing Instrument Co., Ltd, Shangdong, China) under water irrigation. Both halves of the sectioned specimens were polished on a TegraPol-21 polisher (Struers, Copenhagen, Denmark) with progressively finer silicon carbide paper from 1200, 2400 to 4000 grit (Struers, Copenhagen, Denmark) and ultrasonically cleaned for 1 min in water between each polishing session. Final polishing was performed with 9 µm and 1 µm diamond suspension (DP Suspension P, Struers, Copenhagen,Denmark) for 5 min each, and ultrasonically cleaned.

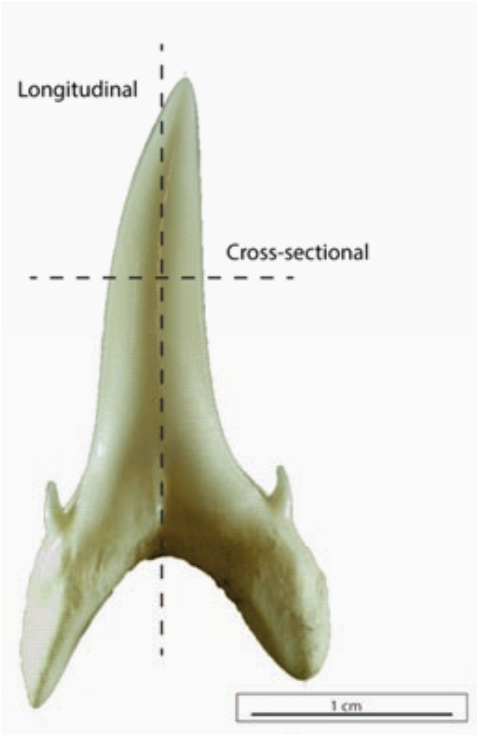

Figure 1. Longitudinal and cross-sectional planes in the teeth of the sand tiger shark.

Scanning electron microscopy (SEM) observations

One longitudinal half of each specimen was used for SEM observations of the microstructure of enameloid and dentine. Specimens were etched using a dental etchant (Scotchbond, 3M ESPE, St Paul, USA) for 30 seconds, ultrasonically cleaned in distilled water for 1 min, and carbon coated before SEM observation. A field emission SEM (JEOL 6700 FESEM, JEOL, Tokyo, Japan) was employed for observation, operating at 5 kV and 10 µA. The specimens were then cross-sectioned (Fig. 1) and polished and etched as previously described in order to obtain cross-sectional images. Magnification in the SEM ranged from 120X to 2500X.

Raman spectroscopy

One of the longitudinally cut and polished halves of each specimen was used for Raman microscopy analysis. Measurements were carried out using a Senterra infinity 1 Raman microscope (Bruker Optics, Germany) with 785nm incident laser at 25mW power, 20x objective and 50 µm aperture to give a 5 µm spot size. Each spectrum produced was a combination of 60 five-second co-additions collected using OPUS 6.5 software (Bruker Optics,

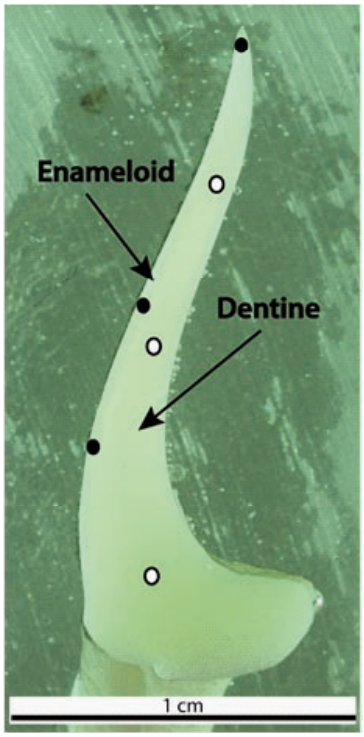

Figure 2. Longitudinal section of a sand tiger shark tooth showing the approximate location of the nanoindentation testing in the enameloid (black dots) and dentine (white dots).

Germany). The resulting Raman spectra were analysed by two methods: principal component analysis (PCA) and peak analysis.

PCA was calculated on the Raman spectra over the spectral region 260–1800 cm^{-1} using a full cross validation calculation after linear baseline correction and standard normal variate pre-processing to remove non-chemical based spectral variance. The pre-processing and PCA calculation were undertaken using the Unscrambler X 10.3 (Camo, Norway). The variables in this instance were the Raman spectra themselves (variables representing a Raman shift of 260 to 1800 cm^{-1}). PCA is a powerful method to reduce complicated spectra with hundreds of variables into a few components which can be visualised in two or three dimensions. These components can then be interpreted to find what spectral and hence chemical differences are observed between the sample spectra. These differences were of major interest as they were the regions showing what was chemically different between and within the various samples.

The $v_1(PO_4^{3-})$ band was fitted for all spectra which contained phosphate spectral features using the Grams AI 8.0 (Thermoscientific) peak fitting module. The window 990 to 920 cm^{-1} was fitted with a mixed Gaussian and Lorentzian peak function, a linear baseline, low sensitivity and a maximum of 50 iterations. Two peaks were fitted into the $v_1(PO_4^{3-})$ band with the major peak centred at approximately 961 cm^{-1} and the minor band at approximately 950 cm^{-1}. The wavenumber of the major band and its associated full width half maximum (FWHM) were recorded. The wavenumber and FWHM of the $v_1(PO_4^{3-})$ band gave information on the mineral environment such as the order/disorder in the structure and the wavenumber shifts reflected the size of the bioapatite crystalline unit cell. Vibrational assignments for phosphate and protein type bands followed Penel et al. (1997) and Kirchner et al. (1997).

Nanoindentation

The mechanical properties of the sand tiger shark teeth were determined by nanoindentation, using the same specimens subjected to Raman spectroscopy. The indentation experiments were performed using a nano-based indentation system (Ultra Micro-Indentation System, UMIS-2000, CSIRO, Australia) with a calibrated Berkovich indenter (Synton, Switzerland). The finished specimens were mounted on metal bases with a thermoplastic adhesive using a paralleling jig (Leitz, Wetzlar, Germany). For the elastic modulus (E) and hardness (H) tests, 100 indents in an array of 10 × 10 with an interval of 20 µm between indents were performed in areas of enameloid and dentine (Fig. 2), with a peak load of 50mN, held for one second. All nanoindentation tests commenced after a thermal soak (minimum of one hour) in the instrument and thermal drift was deemed to be almost negligible (<0.05 nm/sec) before each experiment. E and H were calculated using IBIS software (Fisher-Cripps laboratories Pty. Ltd, NSW, Australia) based on the method and formulae described by Oliver and Pharr (1992).

Results

Macromorphology

Macroscopic analysis of normal and anomalous sand tiger shark teeth revealed contrasting results (Fig. 3). Normal specimens exhibited the expected tooth morphology, with a well-developed tooth crown consisting of a central cusp and two lateral cusplets. The main cusp was slightly curved lingually. Outer margins of the central cusp and lateral cusplets were smooth and sharp (Fig. 4a and b). The root region was also well-defined, with the two characteristic root lobes separated by a basal concavity.

In the anomalous specimens, the crown height was much reduced and the overall shape did not follow the normal characteristic tooth morphology. Often the tip of the crown was curved and lingually curled. Lateral cusplets were also considerably reduced in size and with blunt margins (Fig. 4c and d). The general morphology of the root of the anomalous specimens was largely similar to what was observed for normal specimens.

SEM observations of microstructure

SEM images of all specimens of sand tiger shark teeth considered normal revealed a triple layered enameloid structure (Fig. 5a). The shiny-layered enameloid (SLE) covered the entire outer surface of the teeth analysed. Internally, two more robust layers were observed. The parallel-bundled enameloid (PBE) was

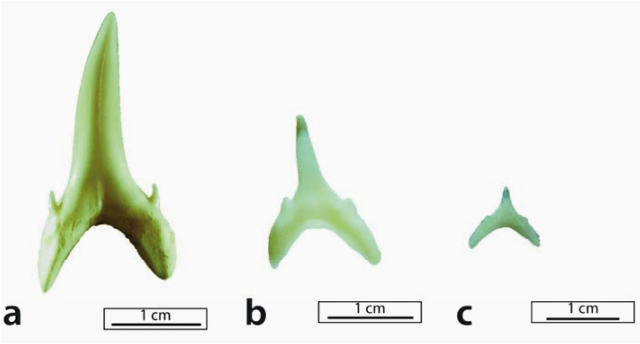

Figure 3. Macromorphology of normal and anomalous teeth of *Carcharias taurus*. a) Normal tooth crown consisting of a lingually curved central cusp and two lateral cusplets and well defined root. b) Anomalous anterior tooth with uncharacteristic shape and reduced crown height. The lateral cusplets are not well defined. Root surfaces have the characteristic lobes as found in the normal teeth. c) Anomalous posterior tooth with blunt margins. Lateral cusplets are not well defined. Scale bar = 1cm.

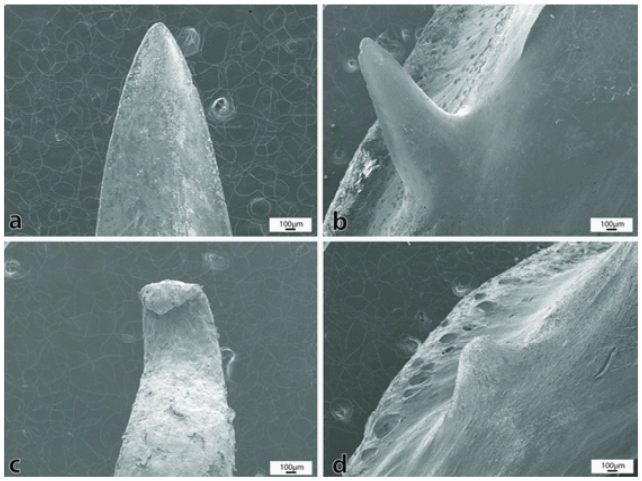

Figure 4. SEM observations of the outer surface of normal and anomalous sand tiger shark teeth. Normal tooth: a) Central cusp. b) Lateral cusplet. Anomalous tooth: c) Central cusp. d) Lateral cusplet. Magnification 35X.

characterised by crystallites oriented in parallel with the bucco-lingual plane in longitudinal sections. The boundary between the SLE and PBE was marked by a sharp and well defined transition (Fig. 5b). The PBE transitioned into tangled-bundled enameloid (TBE) where crystallites were arranged in an interwoven pattern (Fig. 5c). The transition between the PBE and TBE was smooth and it was often difficult to determine specific boundaries. This complex organisation was common near the apex and mid-section of the teeth, whereas at the base of the crown the layers were not as defined.

In cross-section, the crystallites in the PBE layer were perpendicular to the longitudinal plane. The crystallite bundles were separated by radial bundles (RB) that extended from the SLE towards the inner layers of parallel-bundled enameloid (Fig. 5d). Crystallites in the RB layer were oriented at 90° in relation to PBE crystallites.

Analysis of the anomalous soft teeth revealed that little of the crystalline enameloid structure was present in these specimens. However, when present, enameloid was seen in non-contiguous patches covering the outer surface of teeth in longitudinal sections (Fig. 6a). Higher magnification images of these areas revealed isolated patches of parallel-bundled enameloid (PBE), but no outer shiny-layered enameloid or inner tangled-bundled enameloid (Fig. 6b). With the absence of any crystalline structures, enameloid was not observed in cross-sections, with only non-crystalline dentine structures visible (Fig. 6c and d).

Raman spectroscopy

The average Raman spectra from each region measured across the shark teeth showed distinct spectral features associated with the different sectioned tooth domains. The normal specimens had the highest relative intensity of the phosphate type bands at 430, 591, 965, 1052 and 1081 cm^{-1}, indicating fluoroapatite mineral content in the enameloid region of the teeth (Fig. 7). The dentine region of the normal teeth contained lower levels of the phosphate content, and red-shifted with bands typically centred around 428, 588, 961 and 1044 cm^{-1}, which also indicated a fluoroapatite mineral content. The dentine regions also contained protein type bands at 1250, 1455 and 1672 cm^{-1}, which can be assigned as amide III, CH2 scissoring and amide I bands, respectively.

The anomalous teeth had quite different spectra, with the spectra of anomalous tooth 1 having a notable absence of phosphate spectral features (indicating the mineral component of teeth) across all the sampled regions of the tooth. Instead only organic/proteinaceous spectral features were observed (Fig. 8). The posterior tooth (anomalous tooth 2), showed no evidence of mineral content in the tested outer regions of the tooth, and some in the dentine region. The photographic images from within the microscope correspond with the higher mineral content as a lighter region of the tooth, and the higher protein content as a darker region (Figs 7 and 8).

The bandwidth and wavenumber of the $v_1(PO_4^{3-})$ band is sensitive to the bioapatite matrix. The bandwidth is dependent on the order/disorder in the matrix, with increased disorder leading to increased number of stretching environments, hence a broader

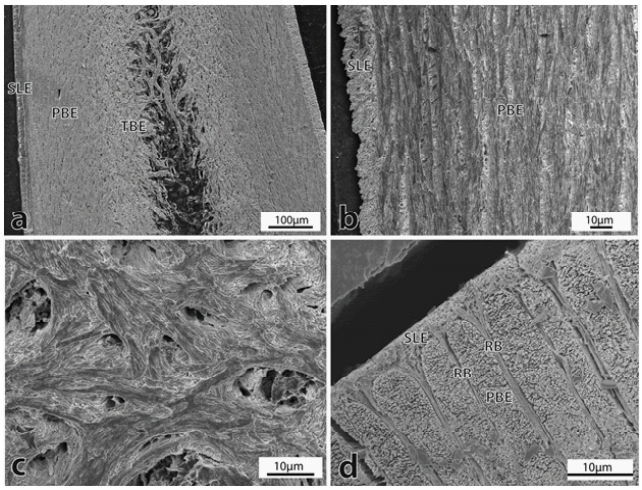

Figure 5. Enameloid ultrastructure of normal sand tiger shark teeth. a) Longitudinal section showing the triple-layered enameloid structure. Magnification 170X. b) Detail of the transition from the shiny-layered enameloid (SLE) to the parallel-bundled enameloid (PBE) layer seen in longitudinal section. Magnification 750X. c) Detail of the tangled-bundled enameloid layer showing the typical interwoven pattern seen in longitudinal section. Magnification 1700X. d) Cross-section showing the outer shiny-layered enameloid (SLE) and the prominent radial bundles (RB) of parallel-bundled enameloid (PBE). Magnification 2500X.

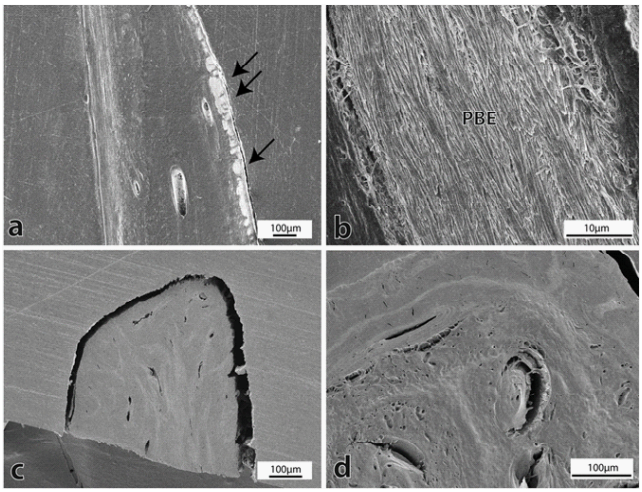

Figure 6. Ultrastructure of anomalous sand tiger shark teeth. a) Longitudinal section showing a few patches of parallel-bundled enameloid (PBE) in the outer surface (arrows). Magnification 90X. b) Detail of one of the patches of parallel-bundled enameloid (PBE) layer seen in longitudinal section. Magnification 2500X. c) Overview of an anomalous sand tiger shark tooth seen in cross-section. Magnification 120X. d) Higher magnification of anomalous sand tiger shark tooth in cross-section showing prominent dentine structures and the lack of enameloid crystalline structures. Magnification 230X.

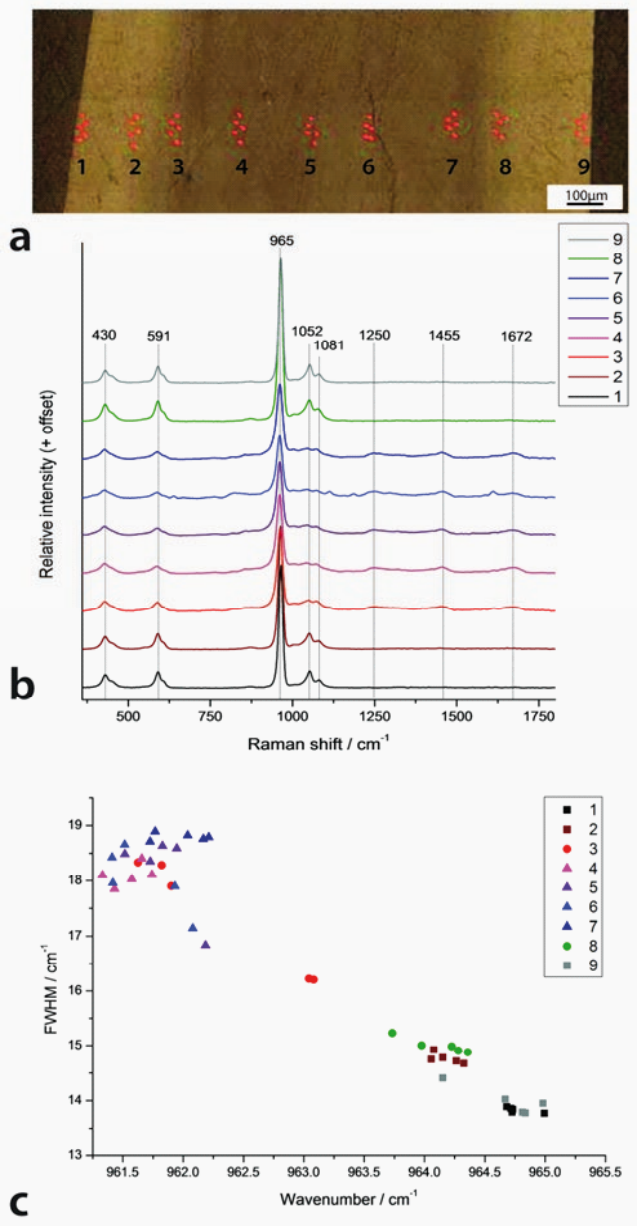

Figure 7. a) Example of multiple sampling regions across the sectioned normal sand tiger shark tooth. b) The associated average Raman spectra from each sample region. c) The FWHM versus wavenumber for the v1(PO43-) band.

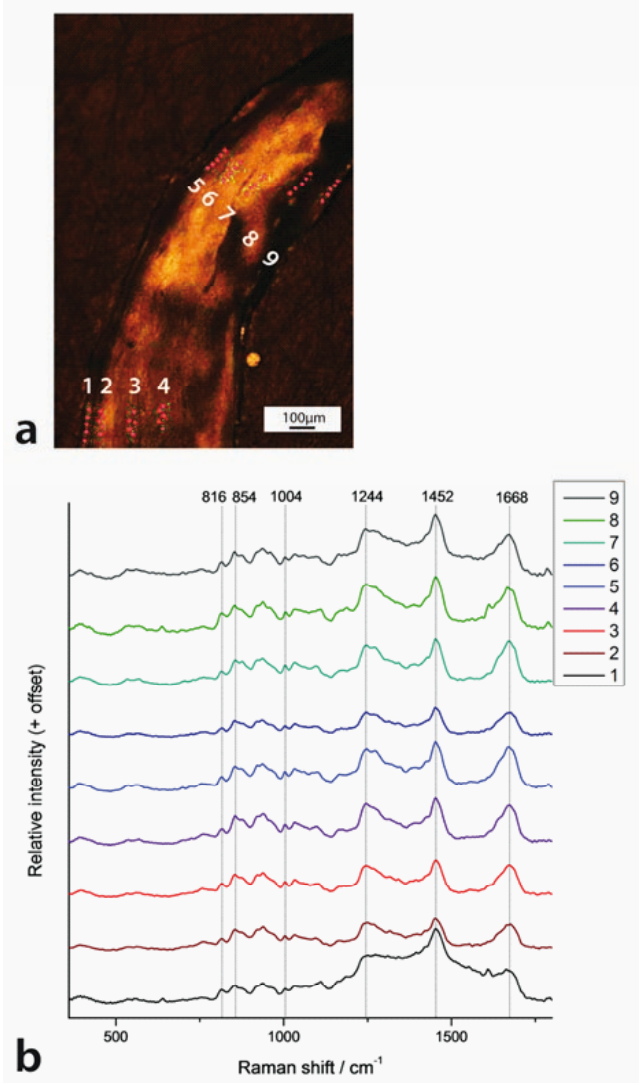

Figure 8. a) Example of multiple sampling regions across the section of anomalous sand tiger shark tooth 1. b) The associated average Raman spectra from each sample region.

bandwidth. The wavenumber is upshifted with a decrease in unit cell, and downshifted with an increased unit cell size, hence the unit cell size changes with different ion substitutions. The $v_1(PO_4^{3-})$ band was fitted for all spectra that contained phosphate features.

The general trend shown for the normal captive specimens (Auckland and Sydney Aquariums) was a narrower bandwidth and upshifted wavenumber for enameloid spectra (FWHM of 11.5–15 cm^{-1}, wavenumber of 964–966.5 cm^{-1}) compared with the dentine spectra (FWHM of 16.5–19 cm^{-1}, wavenumber of 961–963 cm^{-1}) as demonstrated in Figures 7 and 8. The normal wild specimen had a similar pattern, but much closer values between the enameloid (FWHM of 15–16.7 cm^{-1}, wavenumber of 961.5–964.5 cm^{-1}) and dentine regions (FWHM of 17–18.5 cm^{-1}, wavenumber of 960–962 cm^{-1}). Anomalous tooth 1 and the outer region of anomalous tooth 2 were not fitted for the $v_1(PO_4^{3-})$ band due to its absence in the spectra. The anomalous tooth 2 had the $v_1(PO_4^{3-})$ band fitted for the spectra that contained the phosphate band; this corresponded with spectra taken from the dentine region and by the EDJ. The $v_1(PO_4^{3-})$ for the dentine regions was of similar bandwidth and wavenumber to that found in the normal specimens, with a FWHM of 6.5–18 cm^{-1} and wavenumber of 963.1–962.5 cm^{-1}. The $v_1(PO_4^{3-})$ band from the EDJ was within the bandwidth and wavenumber for the normal specimen enameloid values, with a FWHM of 14–15.5 cm^{-1} and wavenumber of 963–964 cm^{-1}.

Principal component analysis (PCA) of the teeth spectra was undertaken to better understand the variance within and between the different specimens. The spectra tended to cluster into three major groups along PC1. The groupings were consistent with enameloid samples containing mineral signals, dentine samples containing mineral and proteinaceous signals and anomalous samples with only protein type signals (Fig. 9a). The

slight differences between the captive and wild-type samples, demonstrated by separation in PC2 space (Fig. 9a), are associated with differences in the mineral structure.

The first principal component accounted for 90% of the total variance between samples and separated the spectra based on the relative mineral (positive PC1 space) and protein (negative PC1 space) content, as seen in the loadings (Fig. 9b). The second PC plotted differences in the apatite, with the shifting of the $v_1(PO_4^{3-})$ band as the dominant separating feature (Fig. 9b). Separation in PC2 space was attributed to the level of fluoridation in the fluoroapatite with positive PC2 having lower levels of fluoridation (downshifted $v_1(PO_4^{3-})$) than negative PC2 space (Fig. 9b).

Nanoindentation

Elastic modulus

Nanoindentation testing was performed on different regions of both the enameloid and dentine of the five specimens tested. The mean enameloid elastic modulus of all three normal teeth was 75.92±3.4 GPa, while the outer layers of the two anomalous teeth had a mean elastic modulus of 7.81±3.27 GPa. The mean elastic modulus of the dentine of the normal and anomalous teeth was very similar at 25.66±2.14 GPa and 25.34±1.54 GPa respectively (Table 1).

Hardness

The hardness values of enameloid of the normal teeth followed the same trend with the mean enameloid hardness of all three normal teeth at 3.27±0.41 GPa. The outer layers of the two anomalous teeth had mean hardness values of 0.39±0.25 GPa.

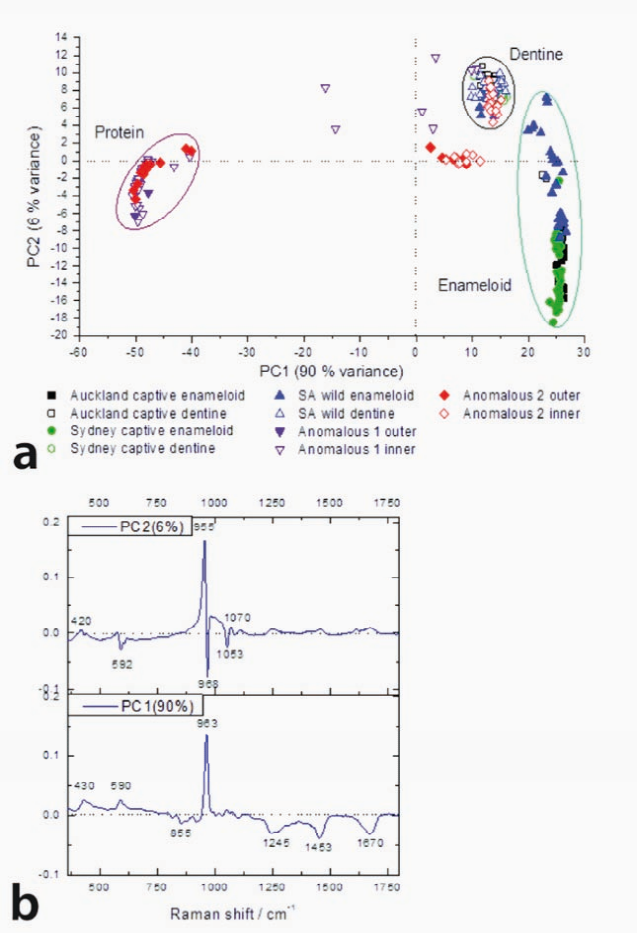

Figure 9. a) Scores plot of the first two PCs (96% variance between samples) from PCA of all the shark tooth samples excluding those containing epoxy signals. b) The loadings for the first two PCs for all shark teeth spectra (excluding individual spectra with epoxy type features).

Table 1. Results from nanoindentation testing of enameloid and dentine from normal teeth of captive and wild specimens and two anomalous teeth of captive *Carcharias taurus*. The standard deviation of the listed values represents the scatter of data within the different indented regions within each tooth.

	Enameloid		Dentine	
	E (GPa)	H (GPa)	E (GPa)	H (GPa)
Normal captive Auckland	78.20 ±8.32	3.6 ±0.53	25.79 ±1.78	0.88 ±0.09
Sydney	77.53 ±6.98	3.38 ±0.55	24.05 ±2.02	0.9 ±0.09
Normal wild South Africa	72.01 ±14.79	2.80 ±0.83	27.04 ±1.44	0.89 ±0.07
	Outer layer		Inner layer	
Anomalous tooth 1	5.49 ±0.55	0.21 ±0.04	24.24 ±2.34	0.81 ±0.09
Anomalous tooth 2	10.12 ±7.12	0.57 ±2.9	26.43 ±1.89	0.85 ±0.08

The mean hardness values of the dentine of normal teeth and the anomalous teeth were also very similar at 0.89±0.01 GPa and 0.83 ±0.03 GPa, respectively (Table 1).

Discussion

Our study investigated microstructural and chemical differences between normal and anomalous teeth found in the sand tiger shark *C. taurus* using SEM, Raman spectroscopy and nanoindentation. Overall, our findings showed that the greatest differences between these two types of teeth resided in the enameloid structure and composition, with lower levels of dissimilarity in the dentine.

The microstructural study of the normal sand tiger shark teeth revealed a triple-layered enameloid structure, as expected for neoselachian sharks (Cuny and Risnes 2005). This typical standard was not observed in the anomalous specimens, with no enameloid or only patches of PBE present. This suggests that these teeth did not have the functional adaptations of force resistance during cutting and gouging predation as normal for sharks with their peculiar microstructural differentiation of tooth enameloid in a triple-layered structure (Gillis and Donoghue 2007).

Previous studies using nanoindentation have shown that shark tooth enameloid has an isotropic behaviour (Enax et al. 2012; Whitenack et al. 2010), which corroborates the findings of this study. The higher hardness and elastic modulus of the enameloid in comparison to the dentine may be due to the higher concentration of fluoroapatite in these areas, which is known to have improved physicochemical and mechanical properties compated to other hydroxyapatites (Gross and Bhadang 2004). A dependence of hardness on the mineral content was also found in human teeth (Cuy et al. 2002). The difference in mechanical properties between the normal tooth enameloid and the outer layers of the anomalous teeth can be attributed to the fact that few mineralised structures were present in these areas to contribute to the stiffness and hardness of the structure. The comparable values of the dentine and inner layers of the anomalous teeth are due to the fact that these areas were observed to be structurally and chemically closer in nature.

The difference in mechanical properties of the normal captive and normal wild teeth may be attributed to the differences in the water chemistry in which the teeth mineralised. This has been shown to be a possible factor in the mechanical properties of

human teeth that come from different geographical areas (Lane and Peach 1997). The influence of different dietary inputs in the mineralisation and mechanical properties of teeth between captive and wild specimens, should not, however, be discarded. Captive animals with skeletal anomalies have depleted levels of vitamins C and E, potassium and zinc, nutrients obtained through the diet and known to affect skeletal mineralisation in other vertebrates (Anderson et al. 2012).

Differences in phosphate structure between the normal wild and captive enameloid could be due to relative fluoridation of the enameloid as they separate along PC2 space (Penel et al. 1997). Positive PC2 space is consistent with a more hydroxyapatite type apatite with the lower wavenumber for $\nu_1(PO_4^{3-})$. Negative PC2 space is consistent with fluoroapatite type apatite with a higher $\nu_1(PO_4^{3-})$. This would suggest that the enameloid may have higher levels of fluoride ions in the apatite matrix, and the dentine regions do not.

The average Raman spectra across each sampled region measured in the normal teeth showed that they had high levels of the phosphate type bands, indicating fluoroapatite in the enameloid. The dentine region of the normal teeth contained lower levels of the apatite component and much higher levels of protein-type spectral features. This was consistent with earlier studies that reported higher mineral component in enameloid consisting of fluoroapatite, and higher protein content in the dentine (Enax et al. 2012; Whitenack et al. 2010). The anomalous tooth 1 spectra indicated no mineral component across all the sampled regions of the tooth, which may mean that the tooth was either totally demineralised or never mineralised in the first place. Anomalous tooth 2 showed no mineral content in the tested outer regions of the tooth. However, the spectra for dentine and EDJ for anomalous tooth 2 were consistent with similar regions in the normal specimens. This suggested that only the outer region of this tooth lacked bioapatite, with only protein constituents observed in this region formed without the mineral component. This was reflected in the elastic modulus and hardness results, where the inner region of this tooth showed similar properties to the normal teeth. Anomalous tooth 1, however, had no bioapatite throughout the tooth structure (detected by visual inspection of the Raman spectra). This was also reflected in the mechanical property results. Previous studies investigating skeletal anomalies in captive *C. taurus* also reported a causal connection between significantly lower material properties and lower mineral content in vertebral centra of affected specimens (Anderson et al. 2012; Huber et al. 2013). It is believed that the chemical and mechanical features observed in the normal specimens used in this study were typical for the species; however, the conclusions are provisional and were made with some caution due to the low sample sizes.

The anomalous teeth studied here are not related to the normal variation in tooth shape observed from the centre to the corners of the jaw or between the upper and lower jaws (monognathic and dignathic heterodonty) (Becker et al. 2000). Although anomalous tooth 2 is morphologically similar to a posterior tooth, the blunt margins of its cusps and soft nature allow its distinction from a normal posterior specimen. The abnormal tooth shape observed in the anomalous specimens were accompanied by deterioration of the enameloid structure and chemical composition, as well as by lower mean values for the mechanical properties. This suggested a pathologic/developmental process affecting those teeth, rather than normal morphological variation.

According to Becker et al. *(*2000), cases of abnormal teeth in sharks have been related to disturbances in tooth development, such as pathological agents affecting the primordial tooth buds. Abnormalities affecting entire tooth files suggest that a long-lasting pathological agent has affected the normal production of teeth; however, short-lived agents with long-lasting effects were also a possible cause. The latter include cases of injury and disease where the insult, or tissue degeneration associated with it, becomes chronic. On the other hand, if an anomaly is observed on a single tooth, it is possible that a short-lived cause such as injury or disease was involved and the condition was later corrected or healed. If the cause of the tooth anomalies is related to a mutation controlling tooth formation, it would happen in the early stages of embryonic development and its effects would last for the lifetime of the animal. In the case of the specimens studied here, collected from the bottom of the aquarium, we could not determine if the anomalous teeth all belonged to the same tooth file or if individual teeth were affected, nor if they belonged to the same individual or to more than one specimen.

Although the morphological, mechanical and chemical differences between the normal and anomalous teeth are quite evident, establishing the aetiology of these differences is still a challenge. Shark enameloid begins to mineralise before the start of dentine mineralisation and enameloid mineralisation generally occurs throughout the layer, with no distinctive front. In addition, odontoblast cell processes extend into the enameloid layer in shark teeth (Cuny and Risnes 2005; Gillis and Donoghue 2007). For the specimens analysed in this study, both normal and anomalous teeth had dentine with similar morphology, mechanical properties and chemical signals. The physical and mechanical integrity of the dentine suggests that the cause of this anomaly was established after the mineralisation of enameloid and dentine, provoking the demineralisation and loss of enameloid but maintaining the soundness of the dentine. It seems unlikely that the establishment of the anomalous condition in the enameloid preceded the mineralisation of dentine. Even though establishing the causes of this condition was not possible at this stage, this study reported and characterised this anomaly in teeth of captive sand tiger sharks, aiming for future contributions of similar cases that could shed some light on the occurrence, aetiology and prevalence of this condition in captive and wild animals.

Acknowledgements

This paper is dedicated to the memory of Professor Jules Kieser, for his valuable contribution to this work and to the lives of the co-authors. We would like to thank Andrew Christie and Craig Thorburn of Kelly Tarlton's Sea Life Aquarium for identifying the anomaly and supplying us with the teeth used in this study. Thanks are also extended to Liz Girvan (OCEM, University of Otago) who provided technical assistance with SEM facilities. C. Loch acknowledges a Sir John Walsh Research Institute Postdoctoral Fellowship.

References

Anderson P.A., Huber D.R., Berzins I.K. (2012) Correlations of capture, transport, and nutrition with spinal deformities in sandtiger sharks, *Carcharias taurus*, in public aquaria. *Journal of Zoo and Wildlife Medicine* 43: 750–758.

Balbino A.C., Antunes M.T. (2007) Pathologic tooth deformities in fossil and modern sharks related to jaw injuries. *Comptes Rendus Palevol* 6: 197–209.

Becker M.A., Chamberlain J.A., Stoffer P.W. (2000) Pathologic tooth deformities in modern and fossil chondrichthians: a consequence of feeding-related injury. *Lethaia* 33: 103–118.

Chan Y.L., Ngan A.H.W., King N.M. (2011) Nano-scale structure and mechanical properties of the human dentine-enamel junction. *Journal of the Mechanical Behavior of Biomedical Materials* 4: 785–795.

Cuny G., Risnes S. (2005) The enameloid microstructure of the teeth of synechodontiform sharks (Chondrichthyes: Neoselachii). *PalArch Series Vertebrate Palaeontology* 3: 8–19.

Cuy J.L., Mann A.B., Livi K.J., Teaford M.F., Weihs, T.P. (2002) Nanoindentation mapping of the mechanical properties of human molar tooth enamel. *Archives of Oral Biology* 47: 281–291.

Dusevich V., Xu C.Q., Wang Y., Walker M.P., Gorski J.P. (2012) Identification of a protein-containing enamel matrix layer which bridges with the

dentine-enamel junction of adult human teeth. *Archives of Oral Biology* 57: 1585–1594.

Enax J., Prymak O., Raabe D., Epple M. (2012) Structure, composition, and mechanical properties of shark teeth. *Journal of Structural Biology* 178: 290–299.

Gardner T.N., Elliott J.C., Sklar Z., Briggs G.A.D. (1992) Acoustic microscope study of the elastic properties of fluorapatite and hydroxyapatite, tooth enamel and bone. *Journal of Biomechanics* 25: 1265–1277.

Gillis J.A., Donoghue P.C.J. (2007) The homology and phylogeny of chondrichthyan tooth enameloid. *Journal of Morphology* 268: 1078–1078.

Goto M. (1991) Evolutionary trends of the tooth structure in Chondrichthyes. In: Suga S., Nakahara, H. (eds.). *Mechanisms and Phylogeny of Mineralization in Biological Systems*. Tokyo: Springer, 447–451.

Gross K.A., Bhadang K.A. (2004) Sinterability, mechanical properties and solubility of sintered fluorapatite-hydroxyapatites. *Key Engineering Materials* 254: 39–42.

Hoenig J.M., Walsh A.H. (1983) Skeletal lesions and deformities in large sharks. *Journal of Wildlife Diseases* 19: 27–33.

Huber D.R., Neveu D.E., Stinson C.M., Anderson P.A., Berzins I. K. (2013) Mechanical properties of sand tiger shark (*Carcharias taurus*) vertebrae in relation to spinal deformity. *Journal of Experimental Biology* 216: 4256–4263.

Imbeni V., Kruzic J.J., Marshall G.W., Marshall S.J., Ritchie R.O. (2005) The dentin–enamel junction and the fracture of human teeth. *Nature Materials* 4: 229–232.

Kirchner M.T., Edwards H.G.M., Lucy D., Pollard A.M. (1997) Ancient and modern specimens of human teeth: a Fourier transform Raman spectroscopic study. *Journal of Raman Spectroscopy* 28: 171–178.

Lane D.W., Peach D.F. (1997) Some observations on the trace element concentrations in human dental enamel. *Biological Trace Element Research* 60: 1–11.

Maisey J.G. (1982) The anatomy and interrelationships of mesozoic hybodont sharks. *American Museum Novitates* 1–48.

Mertinene R.A. (1982) The histology of the teeth of elasmobranchs. *Paleontologicheskii Zhurnal* 1982: 74–82.

Oliver W.C., Pharr G.M. (1992) An improved technique for determining hardness and elastic-modulus using load and displacement sensing indentation experiments. J*ournal of Materials Research* 7: 1564–1583.

Penel G., Leroy G., Rey C., Sombret B., Huvenne J.P., Bres E. (1997) Infrared and Raman microspectrometry study of fluor-fluor-hydroxy and hydroxy-apatite powders. *Journal of Materials Science: Materials in Medicine M* 8: 271–276.

Preziosi R., Gridelli S., Borghetti P., Diana A., Parmeggiani A., Fioravanti M.L., Marcer F., Bianchi I., Walsh M., Berzins I. (2006) Spinal deformity in a sandtiger shark, *Carcharias taurus* Rafinesque: a clinical–pathological study. *Journal of Fish Diseases* 29: 49–60.

Smith M.M., Johanson Z., Underwood C., Diekwisch T.G.H. (2013) Pattern formation in development of chondrichthyan dentitions: a review of an evolutionary model. *Historical Biology* 25: 127–142.

Whitenack L.B., Simkins D.C., Motta P.J. (2011) Biology meets engineering: the structural mechanics of fossil and extant shark teeth. *Journal of Morpholo*gy 272: 169–179.

Whitenack L.B., Simkins D.C., Motta P.J., Hirai M., Kumar A. (2010) Young's modulus and hardness of shark tooth biomaterials. *Archives of Oral Biology* 55: 203–209.

Xue J., Zavgorodniy A.V., Kennedy B.J., Swain M.V., Li W. (2013) X-ray microdiffraction, TEM characterization and texture analysis of human dentin and enamel. *Journal of Microscopy* 251: 144–153.